




Coherent and incoherent magnons induced by strong ultrafast demagnetization in thin permalloy films

Anulekha De ^{1,*} Akira Lentfert,¹ Laura Scheuer,¹ Benjamin Stadtmüller,^{1,2} Georg von Freymann ^{1,3}
Martin Aeschlimann,¹ and Philipp Pirro ^{1,†}

¹*Department of Physics and Research Center OPTIMAS, Rheinland-Pfälzische Technische Universität Kaiserslautern-Landau, 67663 Kaiserslautern, Germany*

²*Institute of Physics, Johannes Gutenberg University Mainz, 55128 Mainz, Germany*

³*Fraunhofer Institute for Industrial Mathematics ITWM, 67663 Kaiserslautern, Germany*



(Received 14 August 2023; revised 7 November 2023; accepted 19 December 2023; published 16 January 2024)

Understanding spin dynamics on femto- and picosecond timescales offers new opportunities for faster and more efficient spintronic devices. Here, we experimentally investigate the coherent spin dynamics after ultrashort laser excitation by performing time-resolved magneto-optical Kerr effect experiments with thin $\text{Ni}_{80}\text{Fe}_{20}$ films. We provide a detailed study of the magnetic field and pump fluence dependence of the coherent precessional dynamics after optical excitation with femtosecond laser pulses. We show that the coherent precession lifetime increases with the strength of the applied magnetic field, which cannot be understood in terms of viscous Gilbert damping of the coherent magnons. Instead, it can be explained by nonlinear magnon interactions and by the change in the fraction of incoherent magnons. This interpretation is in agreement with the observed trends of the coherent magnon amplitude and lifetime as a function of the applied exciting laser fluence. Our results provide insight into the magnetization relaxation processes in ferromagnetic thin films, which are of great importance for further spintronic applications.

DOI: [10.1103/PhysRevB.109.024422](https://doi.org/10.1103/PhysRevB.109.024422)

I. INTRODUCTION

Understanding the microscopic mechanism of laser-induced magnetization dynamics on femto-, pico-, and nanosecond timescales remains still a challenge in condensed matter physics. Using the time-resolved magneto-optical Kerr effect (TR-MOKE), one can directly address the processes responsible for the excitation and relaxation of a magnetic system on their characteristic timescales [1–4]. The pioneering work of Beaupaire *et al.* in 1996 on femtosecond-laser-induced ultrafast demagnetization opened up a new avenue for ultrafast manipulation of the magnetization in magnetic materials [5]. Only a few years later, experiments showed that the ultrafast laser pulses also generate coherent magnons, manifested as precessional dynamics on the nanosecond timescale. The precessional region in magnetic materials is a key parameter for encoding and transferring information in spintronic devices. This regime allows the study of the magnetic anisotropy, damping, and precession frequency of different dynamic modes in continuous thin films and patterned nanostructures [2–4,6–10]. However, the transition between the two regimes of the magnetization dynamics, i.e., the ultrafast demagnetization and the coherent precessional motion on the other side, is very crucial and raises intriguing questions. Many efforts have been made to understand the leading mechanisms as well as to explore their characteristic

timescales. For example, van Kampen *et al.* [2] demonstrated using TR-MOKE that an optical pump pulse can induce coherent uniform spin precession in a ferromagnet. The excitation of these magnons was explained by a transient change in magnetic anisotropy. Later, several works were concerned with exploring the precessional relaxation mechanisms in ferromagnets after ultrafast excitation [11–15]. A recent work showed the excitation of the precession dynamics in ferromagnets with two noncollinear optical pulses, which can affect precessional relaxation mechanisms and damping [16].

In this paper, we take a closer look at the relaxation of the coherent precession induced by ultrafast demagnetization and study in detail the decay time of the measured coherent oscillations as a function of magnetic field and pump fluence. We use femtosecond amplified laser pulses to excite and detect magnetization dynamics in thin permalloy films, including ultrafast demagnetization, fast and slow remagnetization, and precessional dynamics. We observe an unusual magnetic field dependence of the precessional relaxation time which is not in accordance with the expectations from the Gilbert model. Extrinsic contributions such as two-magnon scattering, magnetic anisotropy, and spin pumping [11,17–22] could also affect the magnetization relaxation process and the damping, but we show that these effects can be neglected in our case. Instead, we can relate our observations to nonlinear magnon interactions and the variable contribution of the incoherent magnon background after excitation by a femtosecond optical pulse. Our findings are of general importance for the interpretation of the coherent dynamics measured in similar experiments after ultrafast stimuli.

*ade@rptu.de

†ppirro@rptu.de

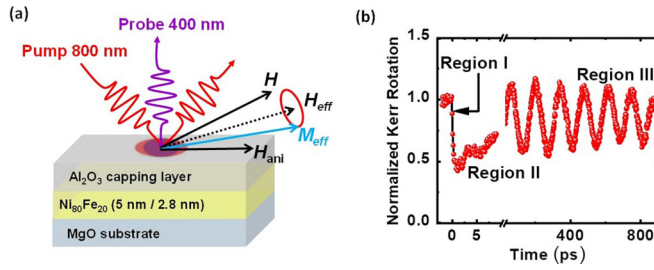


FIG. 1. (a) Schematic diagram of the measurement geometry. (b) Typical experimental TR-MOKE data showing different temporal regimes of the magnetization dynamics for the 5-nm Py sample measured at $\mu_0 H = 113$ mT and $F = 4.6$ mJ cm $^{-2}$.

II. MATERIALS AND METHODS

Permalloy (Ni $_{80}$ Fe $_{20}$, Py) films of 5 and 2.8 nm thickness were deposited on MgO substrates using the molecular beam epitaxy (MBE) technique in an ultrahigh-vacuum chamber. The samples were capped with a 3-nm-thick layer of Al $_2$ O $_3$ to protect them from environmental degradation, oxidation, and laser ablation during the pump-probe experiment using femtosecond laser pulses.

The magnetization dynamics were measured using a TR-MOKE setup based on a two-color, noncollinear optical pump-probe technique. A schematic diagram of the experimental geometry is shown in Fig. 1(a). In this experiment, we use the fundamental output of an amplified femtosecond laser system with wavelength $\lambda = 800$ nm, repetition rate of 1 kHz, and pulse width of ~ 35 fs (Libra; Coherent) as the pump pulse, while its second harmonic with $\lambda = 400$ nm is used to probe the dynamics. The probe is normally incident on the sample, while the pump is incident obliquely ($\sim 30^\circ$) with respect to the surface normal. During the measurements, we have applied a magnetic field inclined at a small angle of $\sim 15^\circ$ to the sample plane. The inclination of the magnetization provides a finite out-of-plane (OOP) demagnetization field which is transiently modified by the pump pulse, inducing a coherent precession of the magnetization [1,2]. This symmetry breaking is important to obtain the same starting phase of the precessional motion for each laser pump pulse to avoid loss of the precession signal in a TR-MOKE experiment averaged over thousands of pump-probe cycles. For a completely in-plane configuration of the external magnetic field, we observe a complete reduction of the precessional signal (see Supplemental Material [23]). To obtain the intrinsic magnetic response, we have performed the measurements for two opposite magnetization directions of the sample and extracted the pure magnetic response from the difference of the two resulting Kerr signals. This is done to eliminate any nonmagnetic signal, i.e., any signal that does not depend of the direction of the sample magnetization [24]. We have used a specially designed photodetector connected to a lock-in amplifier to measure the dynamic Kerr rotation signal. All measurements have been performed under ambient conditions and room temperature.

III. RESULTS AND DISCUSSION

Several processes occur when a femtosecond laser pulse interacts with a ferromagnetic thin film in its saturation con-

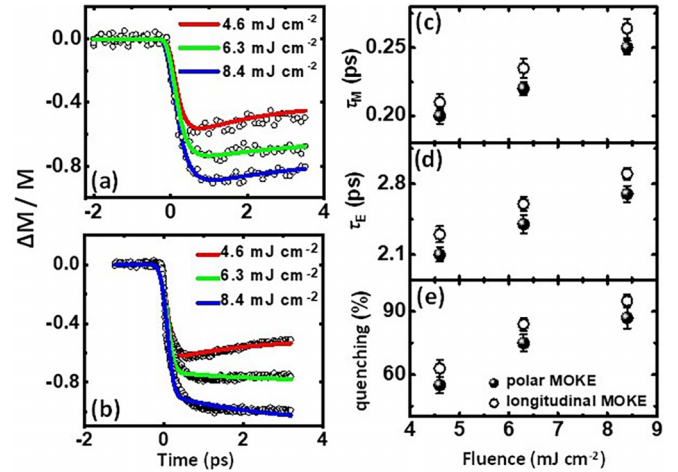


FIG. 2. Ultrafast demagnetization traces at different pump fluences for the 5-nm Py sample in (a) polar and (b) longitudinal MOKE geometries. (c) Demagnetization times τ_M vs pump fluence, (d) fast remagnetization times τ_E vs pump fluence, and (e) quenching vs pump fluence measured in both polar and longitudinal geometries. Solid spheres and open circles represent the data corresponding to polar and longitudinal MOKE geometries, respectively.

dition. First of all, the magnetization of the system is partially or completely lost within hundreds of femtoseconds, which is known as ultrafast demagnetization [5]. This is generally followed by a fast recovery of the magnetization within subpicoseconds to a few picoseconds and a slower recovery within hundreds of picoseconds, known as the fast and slow remagnetization. The slower recovery is accompanied by a precession of the magnetization. On a much longer timescale of a few nanoseconds, the magnetization returns to its initial equilibrium, which can be described phenomenologically by the Gilbert damping [25]. Figure 1(b) shows the representative Kerr rotation data of the 5-nm Py sample for pump fluence $F = 4.6$ mJ cm $^{-2}$ and $\mu_0 H = 113$ mT consisting of three temporal regions of the magnetization dynamics, i.e., the ultrafast demagnetization, the fast remagnetization, and the following slow remagnetization superposed with the damped precession within the time window of 900 ps. The slow remagnetization is mainly due to heat diffusion from the lattice to the substrate and the surroundings. Region I is characterized by the demagnetization time τ_M , and region II is characterized by the fast remagnetization time τ_E . For region III, we characterize the dynamics by the precession frequency f and the precessional relaxation time τ_d .

We start our discussion with the ultrafast demagnetization and fast remagnetization processes of our system to study their dependence on the pump laser fluence and the external magnetic field. In general, the ultrafast demagnetization studies are performed in the longitudinal MOKE geometry. However, to measure the coherent precession of the magnetization, we need to perform measurements in a polar MOKE geometry with a slightly out-of-plane inclined external magnetic field [1,2]. Therefore we first check whether there is a significant difference in the laser-induced ultrafast demagnetization in the two MOKE geometries. Figures 2(a) and 2(b) show the ultrafast demagnetization traces obtained for 5-nm Py in the

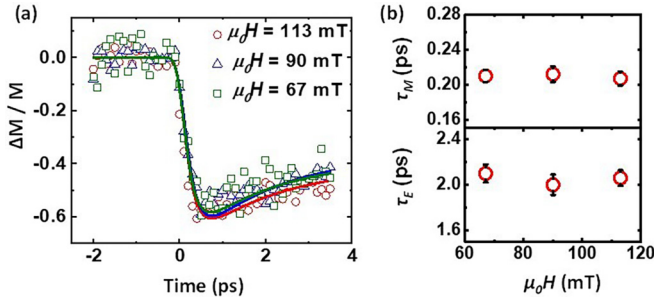


FIG. 3. (a) Ultrafast demagnetization traces for the 5-nm Py sample measured at different values of magnetic field and for fixed $F = 4.6 \text{ mJ cm}^{-2}$. (b) Top: demagnetization times τ_M vs magnetic field. Bottom: fast remagnetization times τ_E vs magnetic field.

polar and longitudinal MOKE geometries, respectively. The pump fluence is varied between 4.6 and 8.4 mJ cm^{-2} by varying the power of the pump pulse. We restrict ourselves to the low-pump-fluence regime to avoid sample damage, and the power of the probe pulse is kept constant at a very low value (approximately a few microwatts) to avoid any additional contribution to the spin dynamics by probe excitation. The ultrafast demagnetization traces for the two geometries show qualitatively similar trends. However, minor discrepancies between the quantitative values obtained from two different geometries arise due to slight differences in the pump spot sizes. The amplitude of the maximum quenching of the Kerr rotation signal increases almost linearly with the laser fluence. Closer inspection of the traces also reveals an increase in the τ_M and τ_E with increasing fluence. To quantify this increase, we fit our demagnetization traces with a phenomenological thermodynamic model, the so-called three-temperature model (3TM) [26], which is obtained by solving the energy rate equation between three different degrees of freedom, e.g., electron, spin, and lattice, under low-pump-fluence conditions (see Supplemental Material [23]).

The fluence-dependent behavior of τ_M , τ_E , and quenching in both MOKE geometries, as shown in Figs. 2(c), 2(d), and 2(e), respectively, is an indication of the spin-flip-process-dominated ultrafast demagnetization in our systems [27–29]. The values of τ_M extracted from our experiments are on the same timescale as previous reports [30] and are too large to represent superdiffusive-transport-driven demagnetization [31]. This is not surprising since the large band gap of the insulating substrate and capping layer prevent any spin transport from Py into the adjacent layers. The values of τ_M , τ_E , and quenching are slightly larger in the longitudinal geometry compared with the polar geometry. However, they do not vary significantly with the applied external magnetic field (as shown in Fig. 3), indicating that, as expected, the comparatively small variations in Zeeman energy as well as the small change in magnetization direction associated with the change in magnetic field strength do not affect the ultrafast magnetization dynamics.

After quantifying the ultrafast demagnetization and fast remagnetization dynamics (regions I and II), we turn to region III, which is characterized by the coherent precessional magnetization dynamics induced by the pump laser pulse. These dynamics in the gigahertz range are generally described by

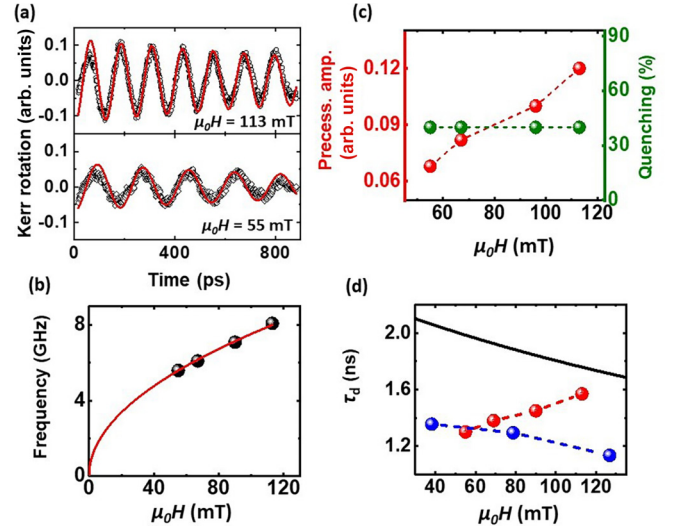


FIG. 4. Magnetic-field-dependent dynamics: (a) Background-subtracted time-resolved Kerr rotation data for the 5-nm Py sample measured at two different magnetic fields and at $F = 4.6 \text{ mJ cm}^{-2}$. The solid curves are fitting curves. (b) Magnetic field dependence of the precession frequency. The solid curve represents the Kittel fit to the data points. (c) Magnetic field dependence of quenching (green) and of precessional amplitude (precess. amp., red). (d) Magnetic field dependence of the precessional relaxation time τ_d measured after ultrafast demagnetization in the TR-MOKE experiment (red), measured using microwave spectroscopy (blue), and determined from analytical calculations (black).

the phenomenological Landau-Lifshitz-Gilbert (LLG) equation [25],

$$\frac{d\vec{M}}{dt} = -\gamma\vec{M} \times \left[\mu_0\vec{H}_{\text{eff}} - \frac{\alpha}{\gamma M_S} \frac{d\vec{M}}{dt} \right], \quad (1)$$

where γ is the gyromagnetic ratio, M_S is the saturation magnetization, α is the Gilbert damping constant, and \vec{H}_{eff} is the effective magnetic field consisting of several field components. The first term on the right-hand side of Eq. (1) accounts for the precession of the magnetization vector \vec{M} around \vec{H}_{eff} . The second term with the first-order time derivative of \vec{M} is the Gilbert damping term [25], which models the transfer of energy and angular momentum of \vec{M} to the surrounding degrees of freedom (relaxation of \vec{M} towards \vec{H}_{eff}). Figure 4(a) shows the background-subtracted time-resolved Kerr rotation data (precessional part) for two different values of the applied magnetic field, fitted with a damped sinusoidal function,

$$M(t) = M(0)e^{-t/\tau_d} \sin(2\pi ft). \quad (2)$$

Here, $M(0)$ is the initial amplitude of the precession, τ_d is the relaxation time of the coherent precession obtained as a fitting parameter, and f is the precession frequency, which can also be extracted directly from the fast Fourier transform (FFT) of the precessional oscillation. Due to the size of the laser spot ($D \sim 500 \text{ }\mu\text{m}$), our measurement basically detects only magnon wave vectors up to approximately $k \sim (\pi/500) \text{ rad }\mu\text{m}^{-1}$, thus essentially only the ferromagnetic resonance (FMR). The effective magnetization M_{eff} , which includes the saturation magnetization and potential additional

out-of-plane anisotropies, is calculated from the magnetic field dependence of the precession frequencies [Fig. 4(b)] and fitting the data points with the Kittel formula [32],

$$f = \frac{1}{2\pi} \sqrt{\omega_H(\omega_H + \omega_M)}, \quad (3)$$

where $\omega_H = \gamma\mu_0 H$, $\omega_M = \gamma\mu_0 M_{\text{eff}}$, H is the externally applied magnetic field, and $\gamma = 1.86 \times 10^{11} \text{ rad s}^{-1} \text{ T}^{-1}$ for Py. Strictly speaking, Eq. (3) is only valid for a completely in-plane magnetized film, but we have verified using micromagnetic simulations that it approximates our experimental situation very well. From the fit, M_{eff} is obtained to be $\sim 700 \pm 25 \text{ kA m}^{-1}$ for 5-nm Py (and $\sim 670 \pm 20 \text{ kA m}^{-1}$ for 2.8-nm Py; see Supplemental Material [23]) measured at $F = 4.6 \text{ mJ cm}^{-2}$.

When studying the excitation of the coherent magnons, points of interest are the dependence of the precession frequency, amplitude, and lifetime on the external conditions. Concerning the amplitude, Fig. 4(c) shows the dependence of quenching and precessional amplitude on the magnetic field for a fixed pump fluence ($F = 4.6 \text{ mJ cm}^{-2}$). As expected, the quenching, which is a measure of the energy initially introduced into the magnetic system, is independent of the applied magnetic field. Surprisingly, at first glance, the precessional amplitude, which is usually considered as a measure for the energy of the coherent oscillations, is strongly dependent on the magnetic field. We interpret the observed increase of the precession amplitude with increasing magnetic field as an increase of the part of the coherent precession that has a well-defined and constant phase relation to the pump pulse. This can be explained by the fact that the static out-of-plane component of the magnetization, which is required for the TR-MOKE experiment to measure the coherent precession [1,2], increases with the strength of the applied bias magnetic field.

Interestingly, we also observe that the precessional relaxation time τ_d , as obtained from TR-MOKE measurements, increases with increasing magnetic field [red spheres in Fig. 4(d)]. This is unexpected if one assumes that Gilbert damping, described by a material parameter (Gilbert damping constant α) is responsible for the decay of the precession. Since Gilbert damping is viscous, it predicts a decrease of the magnon lifetime with increasing frequency, which is equivalent to an increase of the magnetic field strength in the presented geometry. Analytical calculations of the magnon characteristics based on the Gilbert model [33–36] show that the Gilbert-induced lifetime decreases with increasing magnetic field [black solid curve in Fig. 4(d)]. For the analytical calculations, we have assumed an in-plane magnetic field, but we have verified again with micromagnetic simulations that this approximation is well justified. The lifetime (τ_d) of the homogeneous FMR mode for an in-plane-magnetized (the applied in-plane magnetic field is assumed to be H) thin film is calculated using the following expression [36]:

$$\frac{1}{\tau_d} = \alpha \left(\omega_H + \frac{\omega_M}{2} \right). \quad (4)$$

A possible interpretation for this intriguing discrepancy between the lifetimes measured with different excitation mechanisms could be the contribution of non-Gilbert damping

mechanisms. One of these is the so-called two-magnon scattering mechanism, where the magnon energy is redistributed from the FMR ($k = 0$) to other short-wavelength magnons ($k > 0$) due to defect-induced scattering. Arias and Mills [17] developed a theory describing the contributions of two-magnon scattering to the FMR linewidth. The two-magnon process is linear in magnon amplitude; thus the broadening of the FMR linewidth is independent of the magnon amplitude. Woltersdorf *et al.* showed, using TR-MOKE experiments, that different capping layers can affect spin relaxation and damping of Fe films in different ways [19]. They also showed the increase of relaxation time or decrease of damping with increasing magnetic field for Cu-capped Fe films and interpreted it in terms of two-magnon scattering. Liu *et al.* [21] showed that the effective damping constant decreases with the increasing magnetic field, suggesting a contribution of magnetic anisotropy to the enhanced damping. Some other reports have also discussed the enhancement of damping with decreasing magnetic fields due to two-magnon scattering, magnetic anisotropy, or spin pumping effects [11,20,22].

To clarify a possible contribution of two-magnon scattering from defects at surfaces and interfaces [17,18] to the measured decay, we performed additional independent measurements of the FMR lifetime using inductive microwave spectroscopy measured with a vector network analyzer (VNA). This technique is known to be sensitive to linewidth broadening induced by two-magnon scattering [37]. From the inverse of the measured FMR frequency linewidth, we estimate the lifetime of the magnons [blue spheres in Fig. 4(d)] including effects of the inhomogeneous broadening. Thus these values can be considered as a lower bound of the FMR lifetime. A fit to the VNA-measured linewidth shows that the Gilbert damping parameter in the relevant frequency range is $\alpha_{\text{FMR}} = 0.006$ (see Supplemental Material [23] and Ref. [38]). This value of damping has been used for the analytical calculations [α in Eq. (4), black curve in Fig. 4(d)], giving the upper estimate of the FMR lifetime. As expected, this calculated maximum lifetime is larger compared with the experimental results obtained from both measurements. The direct FMR measurements (blue spheres) show a decrease of the lifetime in qualitative accordance with the Gilbert model. The quantitative differences stem from the different influence of the inhomogeneous broadening in the two methods (see Supplemental Material [23]). In addition, a theoretical work [18] predicts that a two-magnon contribution to the linewidth should increase with resonance frequency and magnetic field in our experimental case (small angles of less than 15° to the film's plane). Thus we can conclude that the defect-induced two-magnon scattering is not responsible for the increase in lifetime τ_d observed in our TR-MOKE measurements.

Instead, we interpret the change in lifetime of the coherent precession as follows. Both incoherent and coherent magnons are excited when the sample is hit with a femtosecond laser pulse in the TR-MOKE experiment. The ratio of coherent to incoherent magnons is influenced by the out-of-plane component of the static magnetization, which breaks the symmetry of the system. As in the case of the precession amplitude, a higher external field strength increases the static out-of-plane component and thus the relative proportion of coherent magnons with a defined and constant phase

relationship to the laser pulses. Due to the reduced excitation of the incoherent (or thermal) magnons at higher fields, the dephasing of the precession signal is weaker, leading to a longer lifetime of the measured coherent precession signal. As the external magnetic field decreases, the relative proportion of incoherent to coherent magnons increases, leading to a shorter lifetime. Likewise, the coherent magnons dominate over the incoherent magnons for larger external fields, leading to a longer lifetime. The different ratio of coherent to incoherent or thermal magnons is equivalent to a different ratio of the deterministic effective magnetic field to the effective thermal field introduced by Brown [39]. In fact, in the micromagnetic theory, the thermal magnons are generated by thermal magnetic fields [40]. Since experiments can only measure the thermal magnons, we consider the thermal fields simply as the generators of thermal or incoherent magnons. To further investigate the influence of the temperature, we have also analyzed the magnetic-field-dependent dynamics at higher pump fluence (see Supplemental Material [23]). The precessional relaxation times τ_d as measured by the TR-MOKE experiment show similar trends with magnetic field at higher pump fluence ($F = 6.3 \text{ mJ cm}^{-2}$). Moreover, the values of τ_d are smaller at higher pump fluence (i.e., higher temperature) due to there being more thermally generated incoherent magnons. In contrast to the TR-MOKE measurements, microwave spectroscopy measurements excite mainly coherent magnons, and only a negligible number of thermally generated incoherent magnons are present. This explains the different trends in the lifetime of magnons excited and measured by microwave spectroscopy and the TR-MOKE experiment. Furthermore, we have also calculated the effective damping parameter α_{eff} from TR-MOKE measurements (see Supplemental Material [23] and also Ref. [10]), which shows a decreasing nature with increasing magnetic field (α_{eff} varies from 0.009 to 0.007 as the magnetic field is varied from 55 to 113 mT for 5-nm Py) due to reduced excitation of incoherent or thermal magnons at higher fields. This behavior is again in disagreement with the microwave spectroscopy measurements, which show an invariability of damping with magnetic field. The variation of the effective damping parameter with magnetic field is discussed thoroughly in the Supplemental Material [23]. In general, however, the values of the damping parameter determined from our experiments are consistent with other values reported in the literature [41,42].

Another interesting parameter to study is the influence of the excitation intensity, which in our case is given by the pump fluence, on the coherent dynamics. The background-subtracted time-resolved Kerr rotation data for the 5-nm Py sample measured at different pump fluences (F) are shown in Fig. 5(a). The energy deposited by the pump pulse, in the form of heat within the probed volume, plays a very crucial role in the modification of the local magnetic properties, i.e., the magnetic moment, anisotropy, coercivity, magnetic susceptibility, etc., and the precession frequency can experience a variation with the pump fluence [12,43]. However, we do not observe any significant frequency shift within our experimental fluence range as shown in Fig. 5(b). This also indicates that the temperature of the sample is not significantly increased on longer timescales after the initial, fast remagnetization. Consequently, M_{eff} calculated from Eq. (3) shows no signifi-

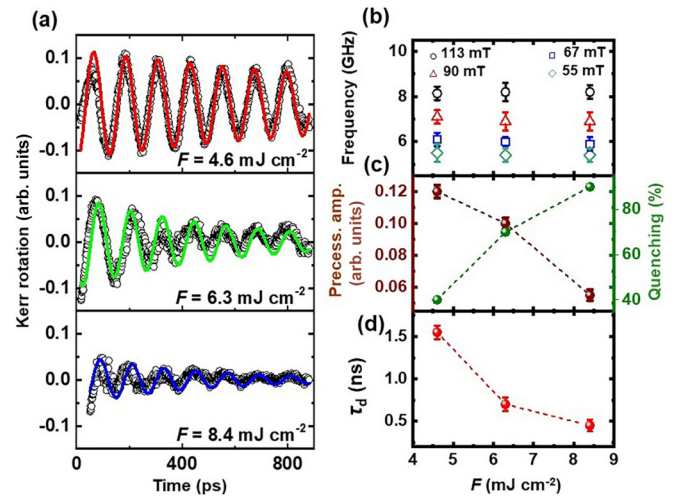


FIG. 5. Pump-fluence-dependent dynamics: (a) Background-subtracted time-resolved Kerr rotation data for the 5-nm Py sample measured at $\mu_0 H = 113 \text{ mT}$ and different pump fluences. The solid curves are fitting curves. (b) Pump fluence dependence of precessional frequencies at $\mu_0 H = 113 \text{ mT}$. (c) Pump fluence dependence of quenching (green) and precessional amplitude (brown). The pump-fluence-dependent quenching plotted here (green) is the same as that plotted with solid spheres in Fig. 2(c). (d) Pump fluence dependence of precessional relaxation time τ_d measured after ultrafast demagnetization in the TR-MOKE experiment.

cant dependence on F within our experimental fluence range. Thus we conclude that as the pump fluence increases, there is no further change in the anisotropy field that can modify the effective magnetization of the system to this extent [21]. Figure 5(c) shows that the quenching increases with pump fluence as expected. However, although the initial quenching is a measure of the absorbed energy and thus the source of coherent precession, the precession amplitude decreases with fluence. The precessional relaxation time τ_d decreases [Fig. 5(d)] and the effective damping parameter increases (see Supplemental Material [23]) with increasing pump fluence. The decrease of both precession amplitude and precessional relaxation time and increase of effective damping with increase of pump fluence can be explained by the dephasing of the magnons due to nonlinear magnon-magnon interactions. These interactions generally increase with an increase in the total magnon population (incoherent and coherent), which we believe is proportional to the quenching. In addition, the probability of excitation of incoherent (or thermal) magnons relative to coherent magnons increases with the increase of disorder in the system and thus with the quenching or pump fluence.

IV. SUMMARY

In summary, the spin dynamics on different timescales in thin $\text{Ni}_{80}\text{Fe}_{20}$ films have been studied using an all-optical TR-MOKE technique. We study the precession dynamics in the gigahertz range after femtosecond-laser-induced ultrafast demagnetization. The demagnetization time, fast remagnetization time, and magnetization quenching studied in both longitudinal and polar geometries show an increasing trend

with excitation fluence, consistent with a spin-flip-scattering-dominated demagnetization process. On a longer timescale of several hundreds of picoseconds, we observe an increase of the coherent precessional relaxation time with magnetic field or resonance frequency, which cannot be explained by viscous Gilbert damping. Using standard FMR techniques, we conclude that two-magnon scattering is not responsible for this behavior. Instead, we can consistently explain all observed trends by considering the different relative contributions of coherent and incoherent magnons produced in the ultrafast demagnetization process and the nonlinear interaction between them. This interpretation also explains the dependence of the coherent magnon amplitude and relax-

ation time on the excitation fluence. We expect that our results will pave the way for future experimental and theoretical investigations towards a deeper understanding of the photon-to-magnon conversion in ultrafast demagnetization processes.

ACKNOWLEDGMENTS

The authors thank Eva Prinz, Jonas Hofer, and Martin Stiehl for technical assistance. The work was funded by the Deutsche Forschungsgemeinschaft (DFG, German Research Foundation) under Grant No. TRR 173-268565370, Spin+X (Projects No. B11 and No. B03).

-
- [1] G. Ju, A. V. Nurmikko, R. F. C. Farrow, R. F. Marks, M. J. Carey, and B. A. Gurney, Ultrafast time resolved photoinduced magnetization rotation in a ferromagnetic/antiferromagnetic exchange coupled system, *Phys. Rev. Lett.* **82**, 3705 (1999).
- [2] M. van Kampen, C. Jozsa, J. T. Kohlhepp, P. LeClair, L. Lagae, W. J. M. de Jonge, and B. Koopmans, All-optical probe of coherent spin waves, *Phys. Rev. Lett.* **88**, 227201 (2002).
- [3] B. Koopmans, J. J. M. Ruigrok, F. DallaLonga, and W. J. M. de Jonge, Unifying ultrafast magnetization dynamics, *Phys. Rev. Lett.* **95**, 267207 (2005).
- [4] J. Walowski, G. Müller, M. Djordjevic, M. Münzenberg, M. Kläui, C. A. F. Vaz, and J. A. C. Bland, Energy equilibration processes of electrons, magnons, and phonons at the femtosecond time scale, *Phys. Rev. Lett.* **101**, 237401 (2008).
- [5] E. Beaurepaire, J.-C. Merle, A. Daunois, and J.-Y. Bigot, Ultrafast spin dynamics in ferromagnetic nickel, *Phys. Rev. Lett.* **76**, 4250 (1996).
- [6] M. Vomir, L. H. F. Andrade, L. Guidoni, E. Beaurepaire, and J.-Y. Bigot, Real space trajectory of the ultrafast magnetization dynamics in ferromagnetic metals, *Phys. Rev. Lett.* **94**, 237601 (2005).
- [7] J. Bigot, M. Vomir, L. Andrade, and E. Beaurepaire, Ultrafast magnetization dynamics in ferromagnetic cobalt: The role of the anisotropy, *Chem. Phys.* **318**, 137 (2005).
- [8] M. Djordjevic and M. Münzenberg, Connecting the timescales in picosecond remagnetization experiments, *Phys. Rev. B* **75**, 012404 (2007).
- [9] A. Barman, S. Wang, J. D. Maas, A. R. Hawkins, S. Kwon, A. Liddle, J. Bokor, and H. Schmidt, Magneto-optical observation of picosecond dynamics of single nanomagnets, *Nano Lett.* **6**, 2939 (2006).
- [10] J. Walowski, M. D. Kaufmann, B. Lenk, C. Hamann, J. McCord, and M. Münzenberg, Intrinsic and non-local Gilbert damping in polycrystalline nickel studied by Ti:sapphire laser fs spectroscopy, *J. Phys. D: Appl. Phys.* **41**, 164016 (2008).
- [11] M. Djordjevic, G. Eilers, A. Parge, M. Münzenberg, and J. S. Moodera, Intrinsic and nonlocal Gilbert damping parameter in all optical pump-probe experiments, *J. Appl. Phys.* **99**, 08F308 (2006).
- [12] S. Mondal and A. Barman, Laser controlled spin dynamics of ferromagnetic thin film from femtosecond to nanosecond timescale, *Phys. Rev. Appl.* **10**, 054037 (2018).
- [13] S. Mukhopadhyay, S. Majumder, S. N. Panda, and A. Barman, Investigation of ultrafast demagnetization and Gilbert damping and their correlation in different ferromagnetic thin films grown under identical conditions, *Nanotechnology* **34**, 235702 (2023).
- [14] J. Bigot and M. Vomir, Ultrafast magnetization dynamics of nanostructures, *Ann. Phys. (Berlin)* **525**, 2 (2013).
- [15] A. Barman and J. Sinha, *Spin Dynamics and Damping in Ferromagnetic Thin Films and Nanostructures* (Springer, Cham, Switzerland, 2017), 156 pp.
- [16] S. Parchenko, D. Pecchio, R. Mondal, P. M. Oppeneer, and A. Scherz, Gilbert damping control with non-collinear dual optical excitation, [arXiv:2305.00259v2](https://arxiv.org/abs/2305.00259v2).
- [17] R. Arias and D. L. Mills, Extrinsic contributions to the ferromagnetic resonance response of ultrathin films, *Phys. Rev. B* **60**, 7395 (1999).
- [18] P. Landeros, R. E. Arias, and D. L. Mills, Two magnon scattering in ultrathin ferromagnets: The case where the magnetization is out of plane, *Phys. Rev. B* **77**, 214405 (2008).
- [19] G. Woltersdorf, M. Buess, B. Heinrich, and C. H. Back, Time resolved magnetization dynamics of ultrathin Fe(001) films: Spin-pumping and two-magnon scattering, *Phys. Rev. Lett.* **95**, 037401 (2005).
- [20] G. Malinowski, K. C. Kuiper, R. Lavrijsen, H. J. M. Swagten, and B. Koopmans, Magnetization dynamics and Gilbert damping in ultrathin Co₄₈Fe₃₂B₂₀ films with out-of-plane anisotropy, *Appl. Phys. Lett.* **94**, 102501 (2009).
- [21] B. Liu, X. Ruan, Z. Wu, H. Tu, J. Du, J. Wu, X. Lu, L. He, R. Zhang, and Y. Xu, Transient enhancement of magnetization damping in CoFeB film via pulsed laser excitation, *Appl. Phys. Lett.* **109**, 042401 (2016).
- [22] Y. Tserkovnyak, A. Brataas, and G. E. W. Bauer, Enhanced Gilbert damping in thin ferromagnetic films, *Phys. Rev. Lett.* **88**, 117601 (2002).
- [23] See Supplemental Material at <http://link.aps.org/supplemental/10.1103/PhysRevB.109.024422> for the three-temperature model (Sec. S1), the precession dynamics for the 2.8-nm Py sample (Sec. S2), the effect of an in-plane magnetic field (Sec. S3), the precessional relaxation times at higher pump fluence (Sec. S4), and the variation of the effective damping parameter with magnetic field and pump fluence (Sec. S5). The Supplemental Material includes Refs. [10,38,41,42].
- [24] R. Wilks, R. J. Hicken, M. Ali, B. J. Hickey, J. D. R. Buchanan, A. T. G. Pym, and B. K. Tanner, Investigation of ultrafast

- demagnetization and cubic optical nonlinearity of Ni in the polar geometry, *J. Appl. Phys.* **95**, 7441 (2004).
- [25] T. Gilbert, A phenomenological theory of damping in ferromagnetic materials, *IEEE Trans. Magn.* **40**, 3443 (2004).
- [26] F. Dalla Longa, J. T. Kohlhepp, W. J. M. de Jonge, and B. Koopmans, Influence of photon angular momentum on ultrafast demagnetization in nickel, *Phys. Rev. B* **75**, 224431 (2007).
- [27] B. Koopmans, G. Malinowski, F. Dalla Longa, D. Steiauf, M. Fähnle, T. Roth, M. Cinchetti, and M. Aeschlimann, Explaining the paradoxical diversity of ultrafast laser-induced demagnetization. *Nat. Mater.* **9**, 259 (2010).
- [28] T. Roth, A. J. Schellekens, S. Alebrand, O. Schmitt, D. Steil, B. Koopmans, M. Cinchetti, and M. Aeschlimann, Temperature dependence of laser-induced demagnetization in Ni: A key for identifying the underlying mechanism, *Phys. Rev. X* **2**, 021006 (2012).
- [29] M. Krauß, T. Roth, S. Alebrand, D. Steil, M. Cinchetti, M. Aeschlimann, and H. C. Schneider, Ultrafast demagnetization of ferromagnetic transition metals: The role of the Coulomb interaction, *Phys. Rev. B* **80**, 180407(R) (2009).
- [30] M. Cinchetti, M. Sánchez Albaneda, D. Hoffmann, T. Roth, J.-P. Wüstenberg, M. Krauß, O. Andreyev, H. C. Schneider, M. Bauer, and M. Aeschlimann, Spin-flip processes and ultrafast magnetization dynamics in Co: Unifying the microscopic and macroscopic view of femtosecond magnetism, *Phys. Rev. Lett.* **97**, 177201 (2006).
- [31] S. Eich, M. Plötzing, M. Rollinger, S. Emmerich, R. Adam, C. Chen, H. C. Kapteyn, M. M. Murnane, L. Plucinski, D. Steil, B. Stadtmüller, M. Cinchetti, M. Aeschlimann, C. M. Schneider, and S. Mathias, Band structure evolution during the ultrafast ferromagnetic-paramagnetic phase transition in cobalt, *Sci. Adv.* **3**, e1602094 (2017).
- [32] C. Kittel, On the theory of ferromagnetic resonance absorption, *Phys. Rev.* **73**, 155 (1948).
- [33] B. Kalinikos, Excitation of propagating spin waves in ferromagnetic films, *IEE Proc., Part H: Microwaves, Opt. Antennas* **127**, 4 (1980).
- [34] B. A. Kalinikos and A. N. Slavin, Theory of dipole-exchange spin wave spectrum for ferromagnetic films with mixed exchange boundary conditions, *J. Phys. C: Solid State Phys.* **19**, 7013 (1986).
- [35] B. A. Kalinikos, M. P. Kostylev, N. V. Kozhus, and A. N. Slavin, The dipole-exchange spin wave spectrum for anisotropic ferromagnetic films with mixed exchange boundary conditions, *J. Phys.: Condens. Matter* **2**, 9861 (1990).
- [36] D. D. Stancil and A. Prabhakar, Quantum theory of spin waves, in *Spin Waves: Theory and Applications* (Springer, Boston, MA, 2009), pp. 33–66.
- [37] I. Neudecker, G. Woltersdorf, B. Heinrich, T. Okuno, G. Gubbiotti, and C. Back, Comparison of frequency, field, and time domain ferromagnetic resonance methods, *J. Magn. Magn. Mater.* **307**, 148 (2006).
- [38] S. S. Kalarickal, P. Krivosik, M. Wu, C. E. Patton, M. L. Schneider, P. Kabos, and T. J. Silva, Ferromagnetic resonance linewidth in metallic thin films: comparison of measurement methods, *J. Appl. Phys.* **99**, 093909 (2006).
- [39] W. F. Brown, Thermal fluctuations of a single-domain particle, *Phys. Rev.* **130**, 1677 (1963).
- [40] M. Mohseni, A. Qaiumzadeh, A. A. Serga, A. Brataas, B. Hillebrands, and P. Pirro, Bose-Einstein condensation of nonequilibrium magnons in confined systems, *New J. Phys.* **22**, 083080 (2020).
- [41] M. A. W. Schoen, J. Lucassen, H. T. Nembach, T. J. Silva, B. Koopmans, C. H. Back, and J. M. Shaw, Magnetic properties of ultrathin 3d transition-metal binary alloys. I. spin and orbital moments, anisotropy, and confirmation of Slater-Pauling behavior, *Phys. Rev. B* **95**, 134410 (2017).
- [42] A. Ruiz-Calaforra, T. Brächer, V. Lauer, P. Pirro, B. Heinz, M. Geilen, A. V. Chumak, A. Conca, B. Leven, and B. Hillebrands, The role of the non-magnetic material in spin pumping and magnetization dynamics in NiFe and CoFeB multilayer systems, *J. Appl. Phys.* **117**, 163901 (2015).
- [43] S. Mizukami, H. Abe, D. Watanabe, M. Oogane, Y. Ando, and T. Miyazaki, Gilbert damping for various Ni₈₀Fe₂₀ thin films investigated using all-optical pump-probe detection and ferromagnetic resonance, *Appl. Phys. Exp.* **1**, 121301 (2008).